

Dilepton rate from a hot and dense rotating QCD medium

Minghua Wei^{12,*}, Chowdhury Aminul Islam^{1,†} and Mei Huang^{1‡}

¹ *School of Nuclear Science and Technology, University of Chinese Academy of Sciences, Beijing 100049, China and*

² *Institute of High Energy Physics, Chinese Academy of Sciences, Beijing 100049, China*

Using a current-current correlation function (CF) we have calculated the photon polarisation tensor for a rotating hot and dense QCD medium. The spectral function (SF), being related to the CF, has been calculated therefrom. As a spectral property, we further estimated the dilepton rate (DR) from the SF. Our major finding is that both the SF and the DR get enhanced in a rotating medium. We also explore the consequences of the interplay between the angular velocity and other parameters like temperature, chemical potential, etc on different quantities that we calculate.

arXiv:2111.05192v1 [hep-ph] 9 Nov 2021

* weimh@ihep.ac.cn

† chowdhury.aminulislam@ucas.ac.cn

‡ huangmei@ucas.ac.cn

I. INTRODUCTION

It is expected that the deconfined state of quark-gluon plasma (QGP) can be created through heavy-ion collisions (HIC) [1, 2]. The QGP at high temperature is supposed to be present after a few microseconds of the big bang in the early universe and the deconfined dense QCD matter can exist in the core of neutron star [3]. Thus the study and characterization of such quantum chromodynamics (QCD) medium are of great importance.

The QCD medium created in HICs or present in nature can be subjected to different extreme environments, e.g., high temperature and/or density, strong magnetic field and rapid rotation etc [4–6]. It is obvious that the properties of the created medium will be affected by such external conditions, which attracts much interest from the theorists to investigate such a system in detail.

Particularly, in the non-central heavy-ion collision(HIC), large vorticity and strong magnetic field will be generated in the early stage of quark-gluon plasma(QGP). Straightforward computation shows that the magnitude of the magnetic field would reach 10^{18-19} Gauss [7, 8], and simulations from kinetic theory and hydrodynamics [9, 10] indicate that the local vorticity would exceed $0.5fm^{-1}$ with the total angular momentum of QGP at a range of $10^4 - 10^5\hbar$. With the presence of a background magnetic field, the strongly interacting matter shows some nontrivial phenomena, for example, Chiral Magnetic Effect(CME) [7, 11–13], Magnetic Catalysis (MC) in the vacuum [14–16], and Inverse Magnetic Catalysis (IMC) around the critical temperature [17–19]. Just like in a magnetic field [20], many interesting phenomena can occur in a rotating medium as well. We could observe anomalous transport properties like chiral vortical effect [11, 13, 21], chiral vortical wave [22] etc. These anomalous processes can be connected to experimental signals, thus can possibly be observed in experiments like HICs [23]. Apart from these anomalous properties, it is also interesting to observe the effect of rotation on the QCD phase diagram — both on the chiral and deconfinement phase transitions [24–27].

Here, we should keep in mind that having created a QCD medium subjected to such a tremendous amount of angular momentum gives us the liberty of exploring it with a better scope. But the existence of such rotating matter is not confined to HICs alone, rather there are many physical circumstances such as trapped non-relativistic bosonic cold atoms in condensed matter physics [28], rapidly rotating neutron stars [29] which can be a source of such rotating matter.

As compared to the magnetic field effects, the rotation-related effects are electric charge blind, and only involve kinetic properties of the QGP and strong interaction which we are mostly interested in. Experimentally, to screen out the EM effects, neutral particles with finite spin numbers are chosen as carriers of the vorticity polarisation effects. As it is difficult to detect the uncharged particles directly the distribution of their charged daughter particles serves as an alternative observable for the global polarisation effect. With the help of the Λ meson, the average magnitude of the vorticity of QGP had been extracted by the STAR collaboration [30]. In these measurements, the expectation of Λ polarisation as well as the vorticity behaviour of collision energy has been confirmed as well. All the results seem to be understandable by considering the energy shift induced by the vorticity polarisation to spins. However, the theory became a little vague when the K^{*0} and ϕ mesons' measurements were presented in [31]. The mismatch between these measurements indicates the fine structure of hadrons may play a non-negligible role in polarisation processes.

From the experimental side, one important property of heavy-ion collisions is the elliptic flow v_2 , which reflects the initial spatial anisotropy of peripheral collisions transferring into the momentum anisotropy. Another valuable electromagnetic signal such as dilepton or photon production reflects properties of the quark and gluon distributions of the QGP, the advantage of this signal is that once the dilepton and photons are produced, they will escape the medium without significant interaction. Recently it has been found from both the PHENIX experiment at RHIC [32] and the ALICE experiment at the LHC [33] that direct photons show a large elliptic flow, which can be comparable to that of hadrons. This is most puzzling because the photons carry information of early stages and the flow at early times should be small. One natural consideration is that the large photon v_2 or anisotropy might be induced by a large magnitude of magnetic field or rapid vorticity, which will polarize the medium and enhance the anisotropy of the system. It has been investigated how magnetic field will affect the photon elliptic flow v_2 in [34, 35], in this manuscript, we would like to investigate the effect of rotation on dilepton rate (DR). Dilepton pairs originate from the same virtual photon[36].

Now, the DR can be calculated from the correlation functions (CF) and their spectral representations [37]. CFs and their spectral representations have been a reliable tool for exploring the many-particle systems in vacuum [38] as well as in different extreme conditions [39, 40]. The spatial part of the spectral function (SF) can be related with the conductivity [41], whereas the temporal part can capture the response of the conserved density fluctuations [42]. On the other hand, the vector-vector CF and its spectral representation are associated with the dilepton production rate (DR) [39, 40]. Investigations of the rate of such lepton pair produced in the HICs is of real importance, as having a larger mean free path than the system size the dilepton can bring along less contaminated information about the stages at which they are created.

Being a very important quantity the vector-vector current CF, its spectral representation and the DR therefrom

have been extensively explored on numerous occasions in different possible scenarios. It is investigated in the ambit of effective models like Nambu—Jona-Lasinio and its Polyakov loop extended version in Ref.[43] and in the matrix model in Refs. [44, 45]. All these calculations were performed with zero magnetic field. The SF and DR have also been calculated using a basic field theoretical approach for both imaginary [46–48] and real time [49, 50] formalisms. Efforts have also been made to explore the effects of magnetic fields on SF and DR through effective model scenarios [51, 52].

In this paper, we mainly focus on the calculation of vector-vector CF in presence of rotation, which has not been looked into before. From the CF we find its spectral representation and thus can explore the effect of rotation on SF. We observe that the sole impact of the rotation is to increase the strength of the SF when it is varied as a function of the invariant mass scaled with temperature. We also could investigate the impact of the other parameters like the temperature, chemical potential, etc on the SF when intertwined with the rotational effects. For a fixed value of the angular velocity, our observation is that variations of other parameters produce known effects on the SF as in the case of zero rotation.

Once we have the SF, it is straightforward to obtain the DR from therein. We find that the enhancement in the SF due to the rotational effects is also reflected in the DR. We estimate the rate as a ratio to the Born rate, which is nothing but the rate for one loop photon polarisation tensor in absence of rotation. This ratio, we learnt, goes over unity at the low invariant mass region and can be 15 – 20% higher than the usual Born rate. This is indeed an important finding in terms of the DR calculation in HIC and signifies the important role that rotation could play in it.

Our manuscript is organised as follows. In Sec. II we outline the formalism that we work in. Then we give the details of our calculation in Sec. III along with the help of appendices. After that, the result has been discussed in Sec. IV and finally, conclusion is drawn in Sec. V.

II. FORMALISM

In this present study, we have considered a QCD medium under rotation. We calculate the current-current (vector) correlation function (CF) or equivalently the photon polarisation tensor in presence of the rotation. The photon polarisation tensor is depicted in Fig. 1. Once we have the CF, we estimate the spectral function (SF) therefrom. Then using that SF we can calculate the dilepton rate (DR) for a rotating medium. To start with the calculation, we need to write down the quark propagator in presence of rotation. Since the topic of rotating medium is relatively new, we give here a little bit of details about it before getting to the propagator.

To study the SF and other related phenomena in a rotating medium, we adopt a rotating frame with vierbein formalism [10, 53]. In a co-moving frame, vierbein(also called tetrad) can be expressed as: $e^a_\mu = \delta^a_\mu + \delta^a_i \delta^0_\mu v_i$ and $e_a^\mu = \delta_a^\mu - \delta_a^0 \delta_i^\mu v_i$ ($a, \mu = 0, 1, 2, 3$ and $i = 1, 2, 3$). For uniformly rotating frame, $\vec{v} = \vec{\Omega} \times \vec{x}$ will be adopted. As a consequence, tetrad fields give us a metric in rotating frame: $g_{\mu\nu} = \eta_{ab} e^a_\mu e^b_\nu$, where η_{ab} is the metric of Minkowski space-time and γ^a is the flat gamma matrices. Correspondingly, $\bar{\gamma}^\mu = e_a^\mu \gamma^a$ satisfy the Clifford algebra $\{\bar{\gamma}^\mu, \bar{\gamma}^\nu\} = 2g^{\mu\nu}$ in general space-time.

The free Lagrangian for Dirac fermions in the co-rotating frame is given by [10],

$$\mathcal{L} = \bar{\psi}[i\bar{\gamma}^\mu(\partial_\mu + \Gamma_\mu) - M_f]\psi, \quad (1)$$

where M_f is the current mass for particular flavor. The connection Γ_μ given by $\Gamma_\mu = \frac{1}{4} \times \frac{1}{2} [\gamma^a, \gamma^b] \Gamma_{ab\mu}$ describes parallel transportation for a fermion field ψ , where $\Gamma_{ab\mu} = \eta_{ac}(e^c_\sigma G^\sigma_{\mu\nu} e^b_\nu - e^b_\sigma G^\sigma_{\mu\nu} e^a_\nu)$ is called spin connection. Spin connection is determined by the tetrad field uniquely, because $G^\sigma_{\mu\nu}$ is the Christoffel connection associated with metric $g_{\mu\nu} = \eta_{ab} e^a_\mu e^b_\nu$ [24, 53].

In heavy-ion collisions, it is easy to check that the direction of rotation or the total angular momentum is along the out-of-plane direction, i.e., perpendicular to the reaction plane [10, 54]. In this work, reaction plane is represented as x - y plane where x -axis goes along the beam direction and y -axis goes along the impact parameter. Consequently, the direction of rotation is along the z -axis. People can calculate the nonzero terms of spin connection $\Gamma_{ab\mu}$ and combine it with $\bar{\gamma}^\mu = e_a^\mu \gamma^a$. Finally, the free Lagrangian with finite chemical potential under rotation is given by [25]

$$\mathcal{L} = \bar{\psi}[i\gamma^a \partial_a + \gamma^0(\Omega \hat{J}_z + \mu) - M_f]\psi, \quad (2)$$

where μ is chemical potential and J_z is the third component of the total angular momentum $\vec{J} = \vec{x} \times \vec{p} + \vec{S}$. Here, we can extract the third component from the spin operator $\vec{S} = \frac{1}{2} \begin{pmatrix} \vec{\sigma} & 0 \\ 0 & \vec{\sigma} \end{pmatrix}$. It is seen that the angular velocity plays a similar role as the chemical potential.

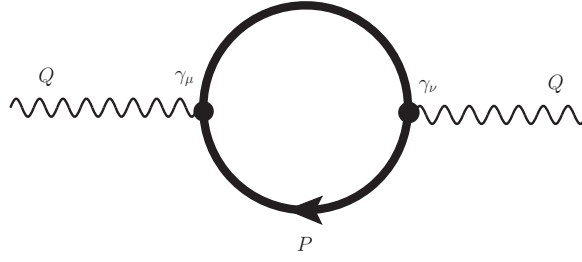


FIG. 1. The photon polarisation tensor.

With all these details, we can now write down the quark propagator in presence of rotation as [55],

$$S(\tilde{r}; \tilde{r}') = \frac{1}{(2\pi)^2} \sum_n \int \frac{dk_0}{2\pi} \int k_t dk_t \int dk_z \frac{e^{in(\phi-\phi')} e^{-ik_0(t-t') + ik_z(z-z')}}{[k_0 + (n + \frac{1}{2})\Omega]^2 - k_t^2 - k_z^2 - M_f^2 + i\epsilon} \\ \times \left\{ \left[[k_0 + (n + \frac{1}{2})\Omega]\gamma^0 - k_z\gamma^3 + M_f \right] \left[J_n(k_tr)J_n(k_tr')\mathcal{P}_+ + e^{i(\phi-\phi')} J_{n+1}(k_tr)J_{n+1}(k_tr')\mathcal{P}_- \right] \right. \\ \left. - i\gamma^1 k_t e^{i\phi} J_{n+1}(k_tr)J_n(k_tr')\mathcal{P}_+ - \gamma^2 k_t e^{-i\phi'} J_n(k_tr)J_{n+1}(k_tr')\mathcal{P}_- \right\}, \quad (3)$$

where $\mathcal{P}_\pm = \frac{1}{2}(1 \pm i\gamma^1\gamma^2)$ are projection operators and $\tilde{r} = (t, r, \theta, z)$ is a point in spacetime. Here we will use Ω to represent angular velocity to distinguish it from real energy ω . In current discussion, we consider $r \ll \Omega^{-1}$ so that causality will be ensured. In real heavy-ion physical process, k_t will be in a finite range. So, $k_tr \ll 1$ will cause that the contribution of higher order Bessel functions are suppressed severely. In fact, z-angular momentum quantum number $n = 0, \pm 1$ will contribute almost entire rotation effect in this framework.

Now using this general fermionic propagator in a rotating medium (3) we can write down the vector current-current CF [43], relevant to the one loop photon self-energy diagram 1, as,

$$\Pi^{ab}(Q) = -i \int d^4\tilde{r} Tr_{Dfc} [i\gamma^a S(0; \tilde{r}) i\gamma^b S(\tilde{r}; 0)] e^{iQ \cdot \tilde{r}}, \quad (4)$$

where Q is the four momentum of external photon line (Fig. 1) and the trace is over Dirac (D), flavour (f) and colour (c) spaces. The traces over the flavour and colour spaces can be performed and the above expression (4) can be rewritten as,

$$\Pi^{ab}(Q) = -iN_f N_c \int d^4\tilde{r} Tr_D [i\gamma^a S(0; \tilde{r}) i\gamma^b S(\tilde{r}; 0)] e^{iQ \cdot \tilde{r}}, \quad (5)$$

where N_f and N_c are the numbers of flavour and colour, respectively; the only trace remaining is the one in the Dirac space. It is to be noted that the CF in Eq. (5) can be easily related to the photon polarisation tensor by appropriately inserting the coupling constant. The SF is also related to the imaginary part of the CF, as

$$\sigma_V(Q) = \frac{1}{\pi} \text{Im} \Pi_a^a(Q), \quad (6)$$

where the Lorentz index a is contracted over. This SF is a quantity of great importance. Many key observables like DR, electrical conductivity, Debye mass etc can be extracted from it. In this work, for a rotating QCD medium, after estimating the SF and discussing it in detail, we extract the DR from it.

The DR can be related to the SF through the well-known relation [43],

$$\frac{dN}{d^4x d^4Q} = \frac{5\alpha^2}{27\pi^2} \frac{1}{M^2} \frac{1}{\exp(\frac{\omega}{T}) - 1} \sigma_V(Q), \quad (7)$$

where the invariant mass of the lepton pair $M^2 = A^2 = \omega^2 - q^2$. Eqs. (6) and (7) are two major equations that we evaluate in the next subsection and discuss in detail in the result section.

III. CALCULATION

A. Diagonal components of the CF

In this subsection, we start with calculating the components of the CF, which will eventually give us the total of it. We insert the propagator (3) into the CF Eq. (5) and then simplify to obtain the diagonal components. The 00 component of the CF is given as,

$$\Pi^{00}(q) = -2N_f N_c \sum_{\eta=\pm 1} \int \frac{d^4 p}{(2\pi)^4} \frac{M_f^2 + \left(p_0 + \frac{\eta\Omega}{2}\right) \left(p_0 + q_0 + \frac{\eta\Omega}{2}\right) + \vec{p} \cdot (\vec{p} + \vec{q})}{\left[\left(p_0 + \frac{\eta\Omega}{2}\right)^2 - \vec{p}^2 - M_f^2\right] \left[\left(p_0 + q_0 + \frac{\eta\Omega}{2}\right)^2 - (\vec{p} + \vec{q})^2 - M_f^2\right]}, \quad (8)$$

where we will put $N_f = 2$ and $N_c = 3$. Similarly, we can obtain the spatial components as well. Then, the finite temperature version of polarisation function can be obtained by replacing p_0 with Matsubara frequency. The explicit expressions of those components are cumbersome, so they will be included in Appendix.A.

After Matsubara Summation calculation with angular velocity Ω in Appendix.B, we obtain simplified expressions for polarisation functions. The 00 component can be read as:

$$\begin{aligned} \Pi^{00}(\omega, \vec{q}) &= \frac{1}{2} N_f N_c \sum_{\eta=\pm 1} \int \frac{d^3 \vec{p}}{(2\pi)^3} \\ &\times \frac{1}{E_p E_k} \left\{ \frac{E_p E_k + \vec{p} \cdot \vec{k} + M_f^2}{\omega - E_p + E_k} \right. \\ &\left[f(E_k - \mu - \frac{\eta\Omega}{2}) - f(E_p - \mu + \frac{\eta\Omega}{2}) - f(E_p + \mu + \frac{\eta\Omega}{2}) + f(E_k + \mu - \frac{\eta\Omega}{2}) \right] \\ &+ [E_p E_k - \vec{p} \cdot \vec{k} - M_f^2] \left(\frac{1}{\omega - E_p - E_k} - \frac{1}{\omega + E_p + E_k} \right) \\ &\times \left[1 - f(E_p - \mu - \frac{\eta\Omega}{2}) - f(E_k + \mu + \frac{\eta\Omega}{2}) \right] \Big\}, \end{aligned} \quad (9)$$

where $k = p + q$ and ω is analytically extended real energy. Comparing it with the ordinary form for 00-component in Ref.([43]), we observe that the rotation effect is embedded in the distribution functions, and the angular velocity Ω acts as an effective chemical potential. However, the rotation effect will affect the spatial part profoundly. It will affect the transverse part and longitudinal part in different ways. Now, the transverse part can be read as:

$$\begin{aligned} \Pi^{11}(\omega, \vec{q}) + \Pi^{22}(\omega, \vec{q}) &= \frac{1}{2} N_f N_c \sum_{\eta=\pm 1} \int \frac{d^3 \vec{p}}{(2\pi)^3} \\ &\times \frac{1}{E_p E_k} \left\{ \frac{2E_p E_k - 2p_z(p_z + q_z) - 2M_f^2}{\omega - E_p + E_k - \eta\Omega} \right. \\ &\times \left[f(E_k - \mu - \frac{\eta\Omega}{2}) - f(E_p - \mu + \frac{\eta\Omega}{2}) - f(E_p + \mu + \frac{\eta\Omega}{2}) + f(E_k + \mu - \frac{\eta\Omega}{2}) \right] \\ &+ [2E_p E_k + 2p_z(p_z + q_z) + 2M_f^2] \left(\frac{1}{\omega - E_p - E_k - \eta\Omega} - \frac{1}{\omega + E_p + E_k + \eta\Omega} \right) \\ &\times \left[1 - f(E_p - \mu + \frac{\eta\Omega}{2}) - f(E_k + \mu + \frac{\eta\Omega}{2}) \right] \Big\}. \end{aligned} \quad (10)$$

Similarly, the longitudinal part can be read as:

$$\begin{aligned}
\Pi^{33}(\omega, \vec{q}) &= \frac{1}{2} N_f N_c \sum_{\eta=\pm 1} \int \frac{d^3 \vec{p}}{(2\pi)^3} \\
&\times \frac{1}{E_p E_k} \left\{ \frac{E_p E_k - [p_x(p_x + q_x) + p_y(p_y + q_y) - p_z(p_z + q_z)] - M_f^2}{\omega - E_p + E_k} \right. \\
&\times \left[f(E_k - \mu - \frac{\eta\Omega}{2}) - f(E_p - \mu - \frac{\eta\Omega}{2}) - f(E_p + \mu + \frac{\eta\Omega}{2}) + f(E_k + \mu + \frac{\eta\Omega}{2}) \right] \\
&+ [E_p E_k + [p_x(p_x + q_x) + p_y(p_y + q_y) - p_z(p_z + q_z)] + M_f^2] \left(\frac{1}{\omega - E_p - E_k} - \frac{1}{\omega + E_p + E_k} \right) \\
&\times \left. \left[1 - f(E_p - \mu - \frac{\eta\Omega}{2}) - f(E_k + \mu + \frac{\eta\Omega}{2}) \right] \right\}. \tag{11}
\end{aligned}$$

Firstly, we should compare transverse and longitudinal parts. We can find an additional Ω term in the denominator of Eq. (10), so it is infeasible to merge the transverse part and longitudinal part as usual. Furthermore, the difference will induce anisotropy of dilepton production in the transverse plane.

B. Imaginary parts

After further simplifications, the details of which can be found in the appendix, we can write down the temporal component of the imaginary part of the self energy. The 00 part can be written as

$$Im\Pi^{00}(\omega, \vec{q}) = \frac{1}{8\pi} N_f N_c \sum_{\eta=\pm 1} \int_{p_-}^{p_+} p dp \frac{4\omega E_p - 4E_p^2 - M^2}{2q E_p} [f(E_p - \mu - \frac{\eta\Omega}{2}) + f(E_p + \mu - \frac{\eta\Omega}{2}) - 1]. \tag{12}$$

Here, $p_{\pm} = \pm \frac{q}{2} + \frac{\omega}{2} \sqrt{1 - \frac{4M_f^2}{\omega^2 - q^2}}$ constrain the integral region. Angular velocity Ω merely appears in the distribution functions, which indicates its impact as an effective chemical potential.

The other three components are calculated in Appendix.C, which are given as:

$$\begin{aligned}
&Im[\Pi^{11}(\omega, \vec{q}) + \Pi^{22}(\omega, \vec{q})] \\
&= -\frac{1}{2} \pi N_f N_c \sum_{\eta=\pm 1} \int_{p_-}^{p_+} \frac{p dp}{(2\pi)^2} \\
&\times \left\{ + \frac{2E_p(\omega - E_p + \eta\Omega) + [(3\frac{q_z^2}{q^2} - 1)(p \cos \theta_1)^2 + (1 - \frac{q_z^2}{q^2}) + 2\frac{q_z^2}{q} p \cos \theta_1] + 2M_f^2}{q E_p} \right. \\
&\times \left. [1 - f(E_p - \mu - \frac{\eta\Omega}{2}) - f(E_p + \mu - \frac{\eta\Omega}{2})] \right\}. \tag{13}
\end{aligned}$$

Here, $p_{\pm}^{\Omega} = \pm \frac{q}{2} + \frac{\omega + \eta\Omega}{2} \sqrt{1 - \frac{4M_f^2}{(\omega + \eta\Omega)^2 - q^2}}$ constrain the integral region and $\cos \theta_1 = \frac{(\omega + \eta\Omega)^2 - 2(\omega + \eta\Omega)\sqrt{p^2 + M_f^2} - q^2}{2pq}$ stands for angle between \vec{p} and \vec{q} . We can find that the rotation affects p_{\pm}^{Ω} and $\cos \theta_1$ terms.

Similarly, the longitudinal part can be read as:

$$\begin{aligned}
&Im\Pi^{33}(\omega, \vec{q}) \\
&= -\frac{1}{2} \pi N_f N_c \sum_{\eta=\pm 1} \int_{p_-}^{p_+} \frac{p dp}{(2\pi)^2} \\
&\times \left\{ \frac{E_p(\omega - E_p) + \frac{1}{2}[(3\frac{q_x^2 + q_y^2 - q_z^2}{q^2} - 1)(p \cos \theta_0)^2 + p^2(1 - \frac{q_x^2 + q_y^2 - q_z^2}{q^2}) + 2\frac{q_x^2 + q_y^2 - q_z^2}{q} p \cos \theta_0] + M_f^2}{q E_p} \right. \\
&\times \left. [1 - f(E_p - \mu - \frac{\eta\Omega}{2}) - f(E_p + \mu - \frac{\eta\Omega}{2})] \right\}. \tag{14}
\end{aligned}$$

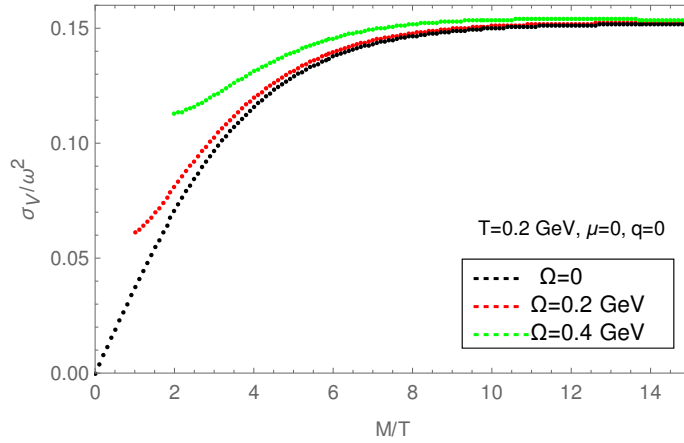


FIG. 2. Spectral function as a function of temperature scaled invariant mass for different values of rotation. The temperature, chemical potential and the external momentum are fixed.

Here, $p_{\pm} = \pm \frac{q}{2} + \frac{\omega}{2} \sqrt{1 - \frac{4M_f^2}{\omega^2 - q^2}}$ constrain the integral region and $\cos \theta_0 = \frac{\omega^2 - 2\omega \sqrt{p^2 + M_f^2} - q^2}{2pq}$. It's obvious and profound that $Im\Pi_a^a(\omega, \vec{q})$ can be expressed as $Im\Pi_a^a(\omega, |\vec{q}|, q_z)$.

IV. RESULTS

A. Spectral function

In this subsection, we will discuss the spectral function (SF) in presence of rotation while taking different combinations of other parameter values. SF is an important quantity by calculating which we can shed light on other important physical quantities.

In Fig. 2 we have displayed the SF as a function of temperature scaled invariant mass (M/T) for different values of the angular velocity, whereas the other parameters are kept fixed. We have used three different values of Ω (0, 0.2 and 0.4 GeV) with temperature and chemical potential kept fixed at 0.2 GeV and 0, respectively. This plot is obtained for zero external momentum. The black dotted line is for zero rotation and as the rotation is introduced the strength of the SF is increased, particularly at lower values of the invariant mass. The higher the values of the rotation (i.e., the angular velocity) the greater the strength of the SF. At high enough values of the invariant mass, the SFs for all values of Ω merge. The increase of the strength in the SF for non-zero values of angular velocities will have an impact on the calculation of the dilepton rate, which is discussed in the next subsection.

In Fig. 3, we have varied the external parameters like temperature and chemical potential, whereas angular velocity is kept fixed at a non-zero value of 0.2 GeV. In the left panel, we have obtained the SF for different values of T and for different values of μ in the right panel. For both the plots, we kept the external momentum to be zero.

This figure (3) is, particularly, drawn with the aim of checking our results for SF with the variations of T and μ for given values of Ω . Here we observe, in the left panel, that as we increase the temperature for given values of other parameters, the SF decreases as a function of M/T . For high enough values of M/T , the SFs with different values of T merge. This behaviour is similar to the zero rotation case. In the same way, we notice that (in the right panel) increasing the values of chemical potential decreases the strength of the SF for other given parameters. This result also conforms with the result for zero rotation where the strength of the SF always decreases with the increase of μ .

Finally, in the discussion of SF, we draw the plot for both non-zero values of Ω and μ shown in Fig. 4, particularly as they have contrasting effects on SF as displayed in Fig. 2 and the right panel of Fig. 3. For this plot, we have used both T and $\mu = 0.2$ GeV and kept the external momentum at zero. It looks qualitatively similar to Fig. 2, that is as we increase the strength of the angular velocity the SF increases for smaller values of invariant mass and merge with the zero rotation SF at sufficiently high values.

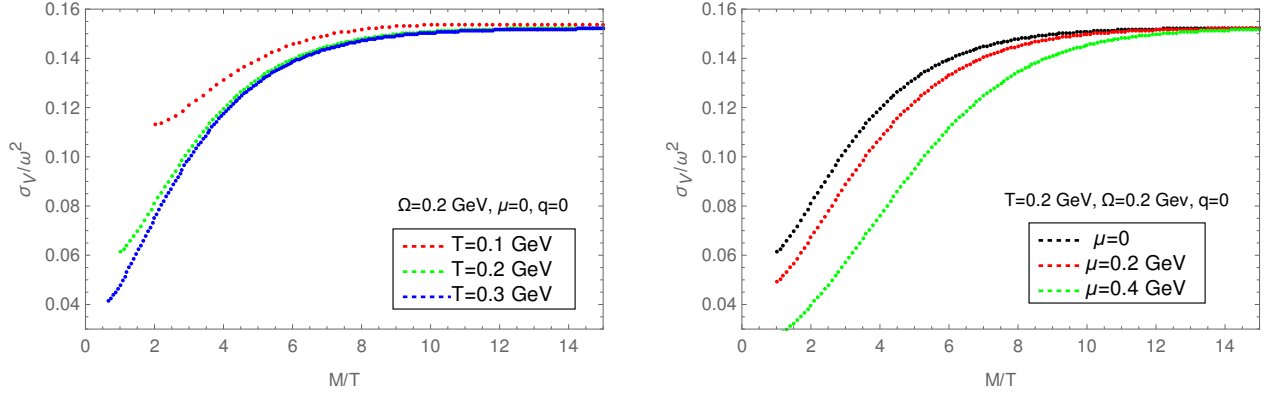


FIG. 3. Left panel: SF as a function of temperature scaled invariant mass for different values of temperature and for fixed values of the angular velocity, chemical potential and the external momentum. Right panel: SF for different values of chemical potential with T , Ω and q being fixed.

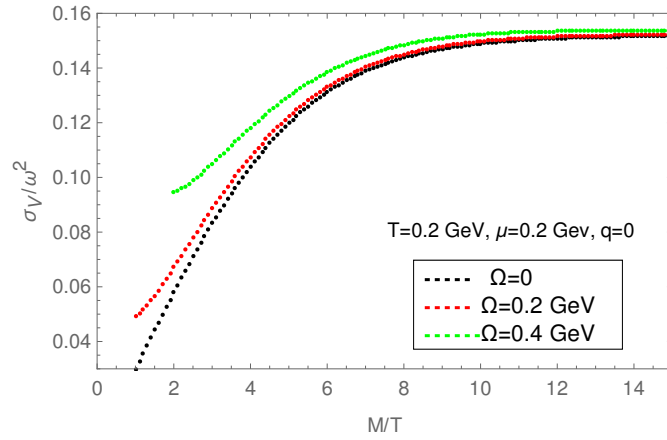


FIG. 4. Spectral function as a function of temperature scaled invariant mass for different values of angular velocity, with nonzero T and μ .

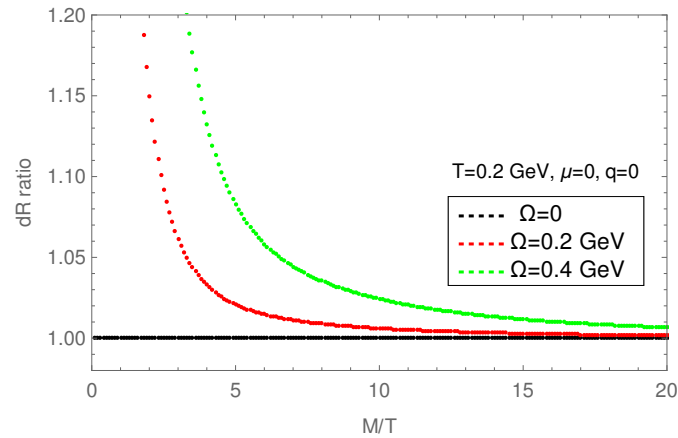


FIG. 5. Ratios of the dilepton rate as a function of temperature scaled invariant mass for different values of rotation. The temperature, chemical potential and the external momentum are fixed.

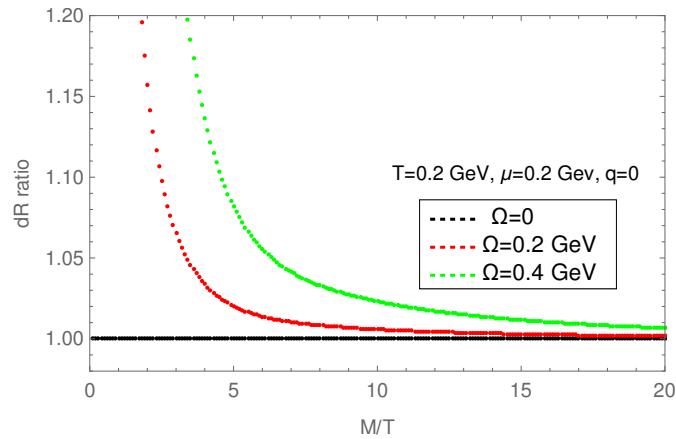


FIG. 6. Ratios of dilepton rate as a function of temperature scaled invariant mass for different values of angular velocity, with nonzero T and μ .

B. Dilepton rate

In this subsection, we describe the results for dilepton rate (DR) which is obtained using the SF obtained in the previous subsection. We are mainly interested here to explore the effect of rotation on the DR. Along with that we also investigate the effects of other parameters on it.

In Fig. 5 we have given the plot for DR as a function of M/T for different values of angular velocity. We have used three different values of Ω as 0, 0.2 and 0.4 GeV, which are represented by the black, red and green points, respectively. Other parameters like temperature, chemical potential and external momentum are kept at fixed values as mentioned in the figure itself. Note that this figure is equivalent to the SF plot in Fig. 2 in terms of the choices of parameters.

The DR is plotted as a ratio between DR at non-zero ω to DR at zero Ω , which is also known as the Born rate. As expected, for zero rotation the DR matches with the known Born rate which is reflected by the black line. For non-zero rotation, there is an enhancement of DR as compared to the Born rate. With the increase of Ω the enhancement gets bigger and appears for higher values of M/T . At the low invariant mass region, this enhancement is $\sim 15 - 20\%$. The nature of this figure can be understood from Fig. 2, since the DR is calculated using the SF.

In Fig. 6 we investigate the effects of both the chemical potential and rotation on the DR. This is particularly interesting because of the contrasting effects of the two agents on the SF as evident from Fig. 2 and the right panel of Fig. 3. The angular velocity enhances the SF whereas the chemical potential diminishes it. It is obtained for three different values of Ω , the values of which along with the other parameters are the same as given in Fig. 4. As expected, the zero rotation rate matches with the Born rate and is represented by the black line. With the increase of Ω , there is an enhancement of DR as compared to the Born rate for non-zero chemical potential.

V. CONCLUSION

Because of its relevance, particularly in heavy-ion collisions (HIC), the consideration of rotation in different QCD related phenomena becomes crucial. Understandably, this stands true for the study of a hot and dense quark-gluon plasma (QGP) which is created in such collisions. Thus, it is very important to characterise a hot and dense QGP in presence of a rotation. In this article, we try to do that by calculating the photon polarisation tensor in presence of a hot and dense QCD medium subjected to a non-zero angular velocity.

We know that the photon polarisation tensor is analogous to the vector current-current correlation function (CF). The CF and its spectral representation are reliable tools to explore many-particle systems. Particularly useful is the dilepton rate (DR) which can be directly estimated from such spectral representation of CF. In this work, our interests revolve around calculating the spectral function (SF) and the DR for a hot and dense QGP medium exposed to a strong rotation. The presence of the rotation makes the whole study much more interesting and the calculation very complicated.

We observe that the SF gets enhanced in presence of a non-zero rotation as compared to the zero cases when plotted as a function of the invariant mass scaled with the temperature. This is obtained while the other parameters like

temperature, chemical potential and external momentum are kept at fixed values. The intertwining effects of the rotation with these parameters on the SF are explored while keeping the strength of the rotation fixed to a non-zero value. In such cases, the qualitative behaviour of the SF remains the same as in the case of zero rotation. Our observation of enhancement in the SF with the increase of the rotational strength could indeed be an interesting finding for the HIC related phenomenology, particularly properties related to the SF.

We explored one such spectral property, namely the DR, which can easily be calculated from the SF. The lepton pairs, as can move freely inside the QCD medium because of their long mean free path, carry information of the stages they are produced to the detector. Thus, their detection can lead us to understand different stages of HICs. Now, the lepton pairs coming out of a rotating QGP must be influenced by the angular velocity. That is what we observe in our study. The enhancement of SF with the increasing angular velocity also gets reflected in the lepton pair production. When the rate is plotted as a ratio to the Born rate we observe an increase of 15 – 20% at the low invariant mass region. This, in our opinion, is an interesting observation which states the importance of consideration of rotational effects in relevant HIC related exercises.

Here, we want to make some final comments regarding similar calculations done in presence of magnetic fields. In the introduction, we drew an analogy between the rotation and the magnetic fields. We talked about different analogous phenomena which can be observed in presence of either of the two. The calculation of DR in presence of a magnetic field also sees enhancement both in the case of lowest Landau level approximation [47] and in arbitrary strength of the fields [48]. Thus, it presents us with a complex and interesting possibility of exploring the rate in presence of both rotation and magnetic field, which we plan to explore in near future.

ACKNOWLEDGMENTS

We thank Kun Xu and Xinyang Wang for their useful discussion. M.H. is supported by the NSFC under Grant Nos. 11725523 and 11735007, Chinese Academy of Sciences under Grant No. XDPB09, the start-up funding from the University of Chinese Academy of Sciences (UCAS), and the Fundamental Research Funds for the Central Universities. CAI was supported by the Chinese Academy of Sciences Presidents International Fellowship Initiative under Grant No. 2020PM0064 and partially by the Fundamental Research Funds for the Central Universities, China.

Appendix A: Components of the polarisation function under rotation

The polarisation function with one loop contribution can be expressed as

$$\Pi^{ab}(q) = -i \int d^4\tilde{r} Tr_{sf} [i\gamma^a S(0; \tilde{r}) i\gamma^b S(\tilde{r}; 0)] e^{iq \cdot \tilde{r}} \quad (A1)$$

where $S(\tilde{r}; \tilde{r}')$ is propagator in rotating medium, its explicit form was shown in Eq.(3). Diagonal components can be calculated as following Ref.([55]). Now, we use $\Pi^{aa}(q)$ for respective components for polarisation functions. $\Pi_a^a(q)$ stands for the summation for components. Rotation will make a difference of the denominator of each $\Pi^{aa}(q)$, so the numerators can not be added up straightforwardly.

For diagonal component:

$$\begin{aligned} \Pi^{00}(q) &= -2N_f N_c \sum_{\eta=\pm 1} \int \frac{d^4p}{(2\pi)^4} \frac{M_f^2 + \left(p_0 + \frac{\eta\Omega}{2}\right) \left(p_0 + q_0 + \frac{\eta\Omega}{2}\right) + \vec{p} \cdot (\vec{p} + \vec{q})}{\left[\left(p_0 + \frac{\eta\Omega}{2}\right)^2 - \vec{p}^2 - M_f^2\right] \left[\left(p_0 + q_0 + \frac{\eta\Omega}{2}\right)^2 - (\vec{p} + \vec{q})^2 - M_f^2\right]} \\ \Pi^{11}(q) &= -2N_f N_c \sum_{\eta=\pm 1} \int \frac{d^4p}{(2\pi)^4} \frac{M_f^2 - \left(p_0 + \frac{\eta\Omega}{2}\right) \left(p_0 + q_0 - \frac{\eta\Omega}{2}\right) - 2p_x(p_x + q_x) + \vec{p} \cdot (\vec{p} + \vec{q})}{\left[\left(p_0 + \frac{\eta\Omega}{2}\right)^2 - \vec{p}^2 - M_f^2\right] \left[\left(p_0 + q_0 - \frac{\eta\Omega}{2}\right)^2 - (\vec{p} + \vec{q})^2 - M_f^2\right]} \\ \Pi^{22}(q) &= -2N_f N_c \sum_{\eta=\pm 1} \int \frac{d^4p}{(2\pi)^4} \frac{M_f^2 - \left(p_0 + \frac{\eta\Omega}{2}\right) \left(p_0 + q_0 - \frac{\eta\Omega}{2}\right) - 2p_y(p_y + q_y) + \vec{p} \cdot (\vec{p} + \vec{q})}{\left[\left(p_0 + \frac{\eta\Omega}{2}\right)^2 - \vec{p}^2 - M_f^2\right] \left[\left(p_0 + q_0 - \frac{\eta\Omega}{2}\right)^2 - (\vec{p} + \vec{q})^2 - M_f^2\right]} \\ \Pi^{33}(q) &= -2N_f N_c \sum_{\eta=\pm 1} \int \frac{d^4p}{(2\pi)^4} \frac{M_f^2 - \left(p_0 + \frac{\eta\Omega}{2}\right) \left(p_0 + q_0 + \frac{\eta\Omega}{2}\right) - 2p_z(p_z + q_z) + \vec{p} \cdot (\vec{p} + \vec{q})}{\left[\left(p_0 + \frac{\eta\Omega}{2}\right)^2 - \vec{p}^2 - M_f^2\right] \left[\left(p_0 + q_0 + \frac{\eta\Omega}{2}\right)^2 - (\vec{p} + \vec{q})^2 - M_f^2\right]} \end{aligned} \quad (A2)$$

Due to symmetric analysis for integration, $\Pi^{11}(q)$ and $\Pi^{22}(q)$ will be equal. This is at zero temperature. To go to nonzero temperature, one needs to make the following transformations,

$$p_0 \rightarrow i\tilde{\omega}_N, \quad q_0 \rightarrow i\nu_n, \quad \int \frac{p_0}{2\pi} \rightarrow iT \sum_N, \quad \tilde{\omega}_N = (2N+1)\pi T. \quad (\text{A3})$$

Here also we can write down the components as well,

$$\Pi^{00}(i\nu_n, \vec{q}) = 2N_f N_c T \sum_N \sum_{\eta=\pm 1} \int \frac{d^3 \vec{p}}{(2\pi)^3} \frac{(i\tilde{\omega}_N + i\nu_n + \frac{1}{2}\eta\Omega + \mu)(\tilde{\omega}_N + \frac{1}{2}\eta\Omega + \mu) + M^2 + (\vec{p} + \vec{q}) \cdot \vec{q}}{\left[(i\tilde{\omega}_N + i\nu_n + \frac{1}{2}\eta\Omega + \mu)^2 - (\vec{p} + \vec{q})^2 - M_f^2\right] \left[(i\tilde{\omega}_N + \frac{1}{2}\eta\Omega + \mu)^2 - \vec{p}^2 - M^2\right]} \quad (\text{A4})$$

$$\begin{aligned} \Pi^{11}(i\nu_n, \vec{q}) = 2N_f N_c T \sum_N \sum_{\eta=\pm 1} \int \frac{d^3 \vec{p}}{(2\pi)^3} \\ - \frac{M_f^2 - \left(i\tilde{\omega}_N + \mu + \frac{\eta\Omega}{2}\right) \left(i\tilde{\omega}_N + \mu + i\nu_n - \frac{\eta\Omega}{2}\right) - p_x(p_x + q_x) + p_y(p_y + q_y) + p_z(p_z + q_z)}{\left[\left(i\tilde{\omega}_N + \mu + \frac{\eta\Omega}{2}\right)^2 - \vec{p}^2 - M_f^2\right] \left[\left(i\tilde{\omega}_N + \mu + i\nu_n - \frac{\eta\Omega}{2}\right)^2 - (\vec{p} + \vec{q})^2 - M_f^2\right]} \end{aligned} \quad (\text{A5})$$

$$\begin{aligned} \Pi^{22}(i\nu_n, \vec{q}) = 2N_f N_c T \sum_N \sum_{\eta=\pm 1} \int \frac{d^3 \vec{p}}{(2\pi)^3} \\ - \frac{M_f^2 - \left(i\tilde{\omega}_N + \mu - \frac{\eta\Omega}{2}\right) \left(i\tilde{\omega}_N + \mu + i\nu_n + \frac{\eta\Omega}{2}\right) + p_x(p_x + q_x) - p_y(p_y + q_y) + p_z(p_z + q_z)}{\left[\left(i\tilde{\omega}_N + \mu - \frac{\eta\Omega}{2}\right)^2 - \vec{p}^2 - M_f^2\right] \left[\left(i\tilde{\omega}_N + \mu + i\nu_n + \frac{\eta\Omega}{2}\right)^2 - (\vec{p} + \vec{q})^2 - M_f^2\right]} \end{aligned} \quad (\text{A6})$$

$$\begin{aligned} \Pi^{33}(i\nu_n, \vec{q}) = 2N_f N_c T \sum_N \sum_{\eta=\pm 1} \int \frac{d^3 \vec{p}}{(2\pi)^3} \\ - \frac{M_f^2 - \left(i\tilde{\omega}_N + \mu + \frac{\eta\Omega}{2}\right) \left(i\tilde{\omega}_N + \mu + i\nu_n + \frac{\eta\Omega}{2}\right) + p_x(p_x + q_x) + p_y(p_y + q_y) - p_z(p_z + q_z)}{\left[\left(i\tilde{\omega}_N + \mu + \frac{\eta\Omega}{2}\right)^2 - \vec{p}^2 - M_f^2\right] \left[\left(i\tilde{\omega}_N + \mu + i\nu_n + \frac{\eta\Omega}{2}\right)^2 - (\vec{p} + \vec{q})^2 - M_f^2\right]} \end{aligned} \quad (\text{A7})$$

Appendix B: Matsubara Summation calculation

Now we give an example for Matsubara Summation calculation with angular velocity Ω :

$$\begin{aligned} & \sum_N \frac{1}{i\tilde{\omega}_N + \omega + \mu - \frac{\Omega}{2} - E_k} \cdot \frac{1}{i\tilde{\omega}_N + \mu + \frac{\Omega}{2} - E_p} \\ &= \sum_N \frac{-i}{(2N+1)\pi T + i(-\omega - \mu + \frac{\Omega}{2} + E_k)} \cdot \frac{-i}{(2N+1)\pi T + i(-\mu - \frac{\Omega}{2} + E_p)} \\ &= - \frac{\coth \frac{1}{2T}(E_k - \omega - \mu + \frac{\Omega}{2} - i\pi T) - \coth \frac{1}{2T}(E_p - \mu - \frac{\Omega}{2} - i\pi T)}{2T[(E_k - \omega - \mu + \frac{\Omega}{2} - i\pi T) - (E_p - \mu - \frac{\Omega}{2} - i\pi T)]} \\ &= \frac{1}{T} \cdot \frac{1}{\omega + E_p - E_k - \Omega} [f(E_p - \mu - \frac{\Omega}{2}) - f(E_k - \mu - \omega + \frac{\Omega}{2})] \end{aligned} \quad (\text{B1})$$

Here, we have applied:

$$\sum_N \frac{1}{N + ix} \frac{1}{N + iy} = \frac{\pi}{x - y} [\coth(\pi x) - \coth(\pi y)] \quad (\text{B2})$$

We can see that a Ω term in denominator. Similarly, we have

$$\begin{aligned}
\sum_N \frac{1}{i\tilde{\omega}_N + \omega + \mu - \frac{\Omega}{2} - E_k} \cdot \frac{1}{i\tilde{\omega}_N + \mu + \frac{\Omega}{2} + E_p} &= \frac{1}{T} \cdot \frac{1}{\omega - E_p - E_k - \Omega} [1 - f(E_p + \mu + \frac{\Omega}{2}) - f(E_k - \mu - \omega + \frac{\Omega}{2})] \\
\sum_N \frac{1}{i\tilde{\omega}_N + \omega + \mu - \frac{\Omega}{2} + E_k} \cdot \frac{1}{i\tilde{\omega}_N + \mu + \frac{\Omega}{2} - E_p} &= \frac{1}{T} \cdot \frac{1}{\omega + E_p + E_k - \Omega} [-1 + f(E_p - \mu - \frac{\Omega}{2}) + f(E_k + \mu + \omega - \frac{\Omega}{2})] \\
\sum_N \frac{1}{i\tilde{\omega}_N + \omega + \mu - \frac{\Omega}{2} + E_k} \cdot \frac{1}{i\tilde{\omega}_N + \mu + \frac{\Omega}{2} + E_p} &= \frac{1}{T} \cdot \frac{1}{\omega - E_p + E_k - \Omega} [-f(E_p + \mu + \frac{\Omega}{2}) + f(E_k + \mu + \omega - \frac{\Omega}{2})]
\end{aligned} \tag{B3}$$

Appendix C: The imaginary part of polarisation function under rotation

In Subsection(III A), whole polarisation functions have been presented. Imaginary part of polarisation function can be extracted by:

$$Im \frac{1}{x + i\epsilon} = -\pi \delta(x) \tag{C1}$$

We write down all the components here. The temporal part is:

$$\begin{aligned}
Im\Pi^{00}(\omega, \vec{q}) &= -\frac{\pi}{2} N_f N_c \sum_{\eta=\pm 1} \int \frac{d^3 \vec{p}}{(2\pi)^3} \\
&\times \frac{1}{E_p E_k} \left\{ [E_p E_k + \vec{p} \cdot \vec{k} + M_f^2] \right. \\
&[f(E_p - \mu - \frac{\eta\Omega}{2}) + f(E_p + \mu - \frac{\eta\Omega}{2})][\delta(\omega + E_p - E_k) - \delta(\omega - E_p + E_k)] \\
&+ [E_p E_k - \vec{p} \cdot \vec{k} - M_f^2] \delta(\omega - E_p - E_k) \\
&\left. \times [1 - f(E_p - \mu - \frac{\eta\Omega}{2}) - f(E_p + \mu - \frac{\eta\Omega}{2})] \right\}
\end{aligned} \tag{C2}$$

The transverse part is:

$$\begin{aligned}
&Im[\Pi^{11}(\omega, \vec{q}) + \Pi^{22}(\omega, \vec{q})] \\
&= -\frac{1}{2} \pi N_f N_c \sum_{\eta=\pm 1} \int \frac{d^3 \vec{p}}{(2\pi)^3} \left\{ \frac{2E_p E_k - 2p_z(p_z + q_z) - 2M_f^2}{E_p E_k} \right. \\
&\times [f(E_k - \mu - \frac{\eta\Omega}{2}) - f(E_p - \mu + \frac{\eta\Omega}{2}) - f(E_p + \mu + \frac{\eta\Omega}{2}) + f(E_k + \mu - \frac{\eta\Omega}{2})] \delta(\omega - E_p + E_k - \eta\Omega) \\
&\left. + \frac{2E_p E_k + 2p_z(p_z + q_z) + 2M_f^2}{E_p E_k} [1 - f(E_p - \mu + \frac{\eta\Omega}{2}) - f(E_k + \mu + \frac{\eta\Omega}{2})] \delta(\omega - E_p - E_k - \eta\Omega) \right\}
\end{aligned} \tag{C3}$$

The longitudinal part is:

$$\begin{aligned}
Im\Pi^{33}(\omega, \vec{q}) &= -\frac{\pi}{2} N_f N_c \sum_{\eta=\pm 1} \int \frac{d^3 \vec{p}}{(2\pi)^3} \\
&\times \frac{1}{E_p E_k} \left\{ [E_p E_k - [p_x(p_x + q_x) + p_y(p_y + q_y) - p_z(p_z + q_z)] - M_f^2] \right. \\
&\times [f(E_p - \mu - \frac{\eta\Omega}{2}) + f(E_p + \mu - \frac{\eta\Omega}{2})][\delta(\omega - E_k + E_p) - \delta(\omega - E_p + E_k)] \\
&+ [E_p E_k + [p_x(p_x + q_x) + p_y(p_y + q_y) - p_z(p_z + q_z)] + M_f^2] \delta(\omega - E_p - E_k) \\
&\left. \times [1 - f(E_p - \mu - \frac{\eta\Omega}{2}) - f(E_p + \mu - \frac{\eta\Omega}{2})] \right\}
\end{aligned} \tag{C4}$$

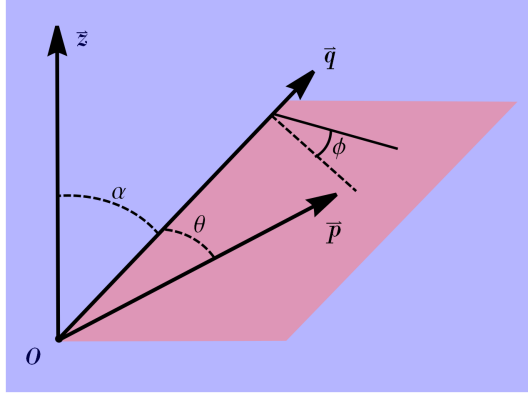


FIG. 7. The angles for integration.

Now, we have to deal with the δ functions and integration in Eq.(C3). Because branch cuts are still confusing, we consider the δ function of $\delta(\omega - E_p - E_k + \eta\Omega)$

For simplification, we will interchange variable of p and k and use an polar coordinate whose polar axis is \vec{q} -axis. For calculation, we will choose a polar coordinate, and \vec{q} will be the polar axis. The new polar axis \vec{q} has an angle α with original z - axis.

As a consequence, p_z and q_z can be represented as following:

$$\begin{cases} q_z = q \cos \alpha \\ p_z = p(\cos \alpha \cos \theta - \sin \alpha \sin \theta \cos \phi) \end{cases} \quad (C5)$$

where θ and ϕ are coordinates for \vec{p} . Relevant angles and vectors are shown in Fig. 7. Eventually, \vec{p} will be integrated, so transverse part can be expressed as a function of q and q_z :

$$\begin{aligned} & Im[\Pi^{11}(\omega, \vec{q}) + \Pi^{22}(\omega, \vec{q})] \\ &= -\frac{1}{2}\pi N_f N_c \sum_{\eta=\pm 1} \int_{p_-^\Omega}^{p_+^\Omega} \frac{p dp}{(2\pi)^2} \\ &\times \left\{ \frac{2E_p(\omega - E_p + \eta\Omega) + [(3\frac{q_z^2}{q^2} - 1)(\frac{(\omega+\eta\Omega)^2 - 2(\omega+\eta\Omega)\sqrt{p^2+M_f^2}-q^2}{2q})^2 + (1 - \frac{q_z^2}{q^2}) + 2\frac{q_z^2}{q} \frac{(\omega+\eta\Omega)^2 - 2(\omega+\eta\Omega)\sqrt{p^2+M_f^2}-q^2}{2q}] + 2M_f^2}{qE_p} \right. \\ &\times \left. [1 - f(E_p - \mu - \frac{\eta\Omega}{2}) - f(E_p + \mu - \frac{\eta\Omega}{2})] \right\} \end{aligned} \quad (C6)$$

It implies a angular distribution on dilepton production. $Im\Pi^{33}(\omega, \vec{q})$ also can be obtain similarly.

-
- [1] B. Muller, THE PHYSICS OF THE QUARK - GLUON PLASMA, Lect. Notes Phys. **225**, 1 (1985).
 - [2] U. W. Heinz and M. Jacob, Evidence for a new state of matter: An Assessment of the results from the CERN lead beam program, (2000), [arXiv:nucl-th/0002042](#).
 - [3] K. Yagi, T. Hatsuda, and Y. Miake, *Quark-gluon plasma: From big bang to little bang*, Vol. 23 (2005).
 - [4] K. Fukushima, QCD matter in extreme environments, *J. Phys. G* **39**, 013101 (2012), [arXiv:1108.2939 \[hep-ph\]](#).
 - [5] D. Kharzeev, K. Landsteiner, A. Schmitt, and H.-U. Yee, eds., *Strongly Interacting Matter in Magnetic Fields*, Vol. 871 (2013).
 - [6] H.-L. Chen, X.-G. Huang, and J. Liao, QCD phase structure under rotation, *Lect. Notes Phys.* **987**, 349 (2021), [arXiv:2108.00586 \[hep-ph\]](#).
 - [7] D. E. Kharzeev, L. D. McLerran, and H. J. Warringa, The Effects of topological charge change in heavy ion collisions: 'Event by event P and CP violation', *Nucl. Phys. A* **803**, 227 (2008), [arXiv:0711.0950 \[hep-ph\]](#).
 - [8] V. Skokov, A. Y. Illarionov, and V. Toneev, Estimate of the magnetic field strength in heavy-ion collisions, *Int. J. Mod. Phys. A* **24**, 5925 (2009), [arXiv:0907.1396 \[nucl-th\]](#).
 - [9] F. Becattini, F. Piccinini, and J. Rizzo, Angular momentum conservation in heavy ion collisions at very high energy, *Phys. Rev. C* **77**, 024906 (2008), [arXiv:0711.1253 \[nucl-th\]](#).
 - [10] Y. Jiang, Z.-W. Lin, and J. Liao, Rotating quark-gluon plasma in relativistic heavy ion collisions, *Phys. Rev. C* **94**, 044910 (2016), [Erratum: *Phys. Rev. C* 95, 049904 (2017)], [arXiv:1602.06580 \[hep-ph\]](#).
 - [11] D. Kharzeev and A. Zhitnitsky, Charge separation induced by P-odd bubbles in QCD matter, *Nucl. Phys. A* **797**, 67 (2007), [arXiv:0706.1026 \[hep-ph\]](#).
 - [12] K. Fukushima, D. E. Kharzeev, and H. J. Warringa, The Chiral Magnetic Effect, *Phys. Rev. D* **78**, 074033 (2008), [arXiv:0808.3382 \[hep-ph\]](#).
 - [13] D. E. Kharzeev and D. T. Son, Testing the chiral magnetic and chiral vortical effects in heavy ion collisions, *Phys. Rev. Lett.* **106**, 062301 (2011), [arXiv:1010.0038 \[hep-ph\]](#).
 - [14] S. P. Klevansky and R. H. Lemmer, Chiral symmetry restoration in the Nambu-Jona-Lasinio model with a constant electromagnetic field, *Phys. Rev. D* **39**, 3478 (1989).
 - [15] K. G. Klimenko, Three-dimensional Gross-Neveu model in an external magnetic field, *Teor. Mat. Fiz.* **89**, 211 (1991).
 - [16] V. P. Gusynin, V. A. Miransky, and I. A. Shovkovy, Dimensional reduction and catalysis of dynamical symmetry breaking by a magnetic field, *Nucl. Phys. B* **462**, 249 (1996), [arXiv:hep-ph/9509320](#).
 - [17] G. S. Bali, F. Bruckmann, G. Endrodi, Z. Fodor, S. D. Katz, S. Krieg, A. Schafer, and K. K. Szabo, The QCD phase diagram for external magnetic fields, *JHEP* **02**, 044, [arXiv:1111.4956 \[hep-lat\]](#).
 - [18] G. S. Bali, F. Bruckmann, G. Endrodi, Z. Fodor, S. D. Katz, and A. Schafer, QCD quark condensate in external magnetic fields, *Phys. Rev. D* **86**, 071502 (2012), [arXiv:1206.4205 \[hep-lat\]](#).
 - [19] G. S. Bali, F. Bruckmann, G. Endrodi, F. Gruber, and A. Schaefer, Magnetic field-induced gluonic (inverse) catalysis and pressure (an)isotropy in QCD, *JHEP* **04**, 130, [arXiv:1303.1328 \[hep-lat\]](#).
 - [20] V. A. Miransky and I. A. Shovkovy, Quantum field theory in a magnetic field: From quantum chromodynamics to graphene and Dirac semimetals, *Phys. Rept.* **576**, 1 (2015), [arXiv:1503.00732 \[hep-ph\]](#).
 - [21] D. T. Son and P. Surowka, Hydrodynamics with Triangle Anomalies, *Phys. Rev. Lett.* **103**, 191601 (2009), [arXiv:0906.5044 \[hep-th\]](#).
 - [22] Y. Jiang, X.-G. Huang, and J. Liao, Chiral vortical wave and induced flavor charge transport in a rotating quark-gluon plasma, *Phys. Rev. D* **92**, 071501 (2015), [arXiv:1504.03201 \[hep-ph\]](#).
 - [23] D. E. Kharzeev, J. Liao, S. A. Voloshin, and G. Wang, Chiral magnetic and vortical effects in high-energy nuclear collisions—A status report, *Prog. Part. Nucl. Phys.* **88**, 1 (2016), [arXiv:1511.04050 \[hep-ph\]](#).
 - [24] Y. Jiang and J. Liao, Pairing Phase Transitions of Matter under Rotation, *Phys. Rev. Lett.* **117**, 192302 (2016), [arXiv:1606.03808 \[hep-ph\]](#).
 - [25] X. Wang, M. Wei, Z. Li, and M. Huang, Quark matter under rotation in the NJL model with vector interaction, *Phys. Rev. D* **99**, 016018 (2019), [arXiv:1808.01931 \[hep-ph\]](#).
 - [26] Y. Jiang, Chiral vortical catalysis, (2021), [arXiv:2108.09622 \[hep-ph\]](#).
 - [27] V. V. Braguta, A. Y. Kotov, D. D. Kuznedelev, and A. A. Roenko, Influence of relativistic rotation on the confinement-deconfinement transition in gluodynamics, *Phys. Rev. D* **103**, 094515 (2021), [arXiv:2102.05084 \[hep-lat\]](#).
 - [28] A. L. Fetter, Rotating trapped Bose-Einstein condensates, *Rev. Mod. Phys.* **81**, 647 (2009).
 - [29] E. Berti, F. White, A. Maniopoulou, and M. Bruni, Rotating neutron stars: An Invariant comparison of approximate and numerical spacetime models, *Mon. Not. Roy. Astron. Soc.* **358**, 923 (2005), [arXiv:gr-qc/0405146](#).
 - [30] L. Adamczyk *et al.* (STAR), Global Λ hyperon polarization in nuclear collisions: evidence for the most vortical fluid, *Nature* **548**, 62 (2017), [arXiv:1701.06657 \[nucl-ex\]](#).
 - [31] S. Acharya *et al.* (ALICE), Evidence of Spin-Orbital Angular Momentum Interactions in Relativistic Heavy-Ion Collisions, *Phys. Rev. Lett.* **125**, 012301 (2020), [arXiv:1910.14408 \[nucl-ex\]](#).
 - [32] A. Adare *et al.* (PHENIX), Observation of direct-photon collective flow in $\sqrt{s_{NN}} = 200$ GeV Au+Au collisions, *Phys. Rev. Lett.* **109**, 122302 (2012), [arXiv:1105.4126 \[nucl-ex\]](#).
 - [33] D. Lohner (ALICE), Measurement of Direct-Photon Elliptic Flow in Pb-Pb Collisions at $\sqrt{s_{NN}} = 2.76$ TeV, *J. Phys. Conf. Ser.* **446**, 012028 (2013), [arXiv:1212.3995 \[hep-ex\]](#).
 - [34] X. Wang, I. A. Shovkovy, L. Yu, and M. Huang, Ellipticity of photon emission from strongly magnetized hot QCD plasma,

- Phys. Rev. D* **102**, 076010 (2020), [arXiv:2006.16254 \[hep-ph\]](#).
- [35] X. Wang and I. Shovkovy, Photon polarization tensor in a magnetized plasma: absorptive part, (2021), [arXiv:2103.01967 \[nucl-th\]](#).
 - [36] P. Salabura and J. Stroth, Dilepton radiation from strongly interacting systems, *Prog. Part. Nucl. Phys.* **120**, 103869 (2021), [arXiv:2005.14589 \[nucl-ex\]](#).
 - [37] D. Forster, *Hydrodynamics Fluctuation, Broken Symmetry and Correlation Function* (CRC Press, 2018).
 - [38] R. M. Davidson and E. Ruiz Arriola, Mesonic correlation functions in the NJL model with vector mesons, *Phys. Lett. B* **359**, 273 (1995).
 - [39] J. I. Kapusta and C. Gale, *Finite-temperature field theory: Principles and applications*, Cambridge Monographs on Mathematical Physics (Cambridge University Press, 2011).
 - [40] M. L. Bellac, *Thermal Field Theory*, Cambridge Monographs on Mathematical Physics (Cambridge University Press, 2011).
 - [41] A. Francis and O. Kaczmarek, On the temperature dependence of the electrical conductivity in hot quenched lattice QCD, *Prog. Part. Nucl. Phys.* **67**, 212 (2012), [arXiv:1112.4802 \[hep-lat\]](#).
 - [42] T. Kunihiro, Quark number susceptibility and fluctuations in the vector channel at high temperatures, *Phys. Lett. B* **271**, 395 (1991).
 - [43] C. A. Islam, S. Majumder, N. Haque, and M. G. Mustafa, Vector meson spectral function and dilepton production rate in a hot and dense medium within an effective QCD approach, *JHEP* **02**, 011, [arXiv:1411.6407 \[hep-ph\]](#).
 - [44] C. Gale, Y. Hidaka, S. Jeon, S. Lin, J.-F. Paquet, R. D. Pisarski, D. Satow, V. V. Skokov, and G. Vujanovic, Production and Elliptic Flow of Dileptons and Photons in a Matrix Model of the Quark-Gluon Plasma, *Phys. Rev. Lett.* **114**, 072301 (2015), [arXiv:1409.4778 \[hep-ph\]](#).
 - [45] Y. Hidaka, S. Lin, R. D. Pisarski, and D. Satow, Dilepton and photon production in the presence of a nontrivial Polyakov loop, *JHEP* **10**, 005, [arXiv:1504.01770 \[hep-ph\]](#).
 - [46] N. Sadooghi and F. Taghinavaz, Dilepton production rate in a hot and magnetized quark-gluon plasma, *Annals Phys.* **376**, 218 (2017), [arXiv:1601.04887 \[hep-ph\]](#).
 - [47] A. Bandyopadhyay, C. A. Islam, and M. G. Mustafa, Electromagnetic spectral properties and Debye screening of a strongly magnetized hot medium, *Phys. Rev. D* **94**, 114034 (2016), [arXiv:1602.06769 \[hep-ph\]](#).
 - [48] A. Das, A. Bandyopadhyay, and C. A. Islam, Lepton pair production from a hot and dense QCD medium in presence of an arbitrary magnetic field, (2021), [arXiv:2109.00019 \[hep-ph\]](#).
 - [49] A. Bandyopadhyay and S. Mallik, Effect of magnetic field on dilepton production in a hot plasma, *Phys. Rev. D* **95**, 074019 (2017), [arXiv:1704.01364 \[hep-ph\]](#).
 - [50] S. Ghosh and V. Chandra, Electromagnetic spectral function and dilepton rate in a hot magnetized QCD medium, *Phys. Rev. D* **98**, 076006 (2018), [arXiv:1808.05176 \[hep-ph\]](#).
 - [51] C. A. Islam, A. Bandyopadhyay, P. K. Roy, and S. Sarkar, Spectral function and dilepton rate from a strongly magnetized hot and dense medium in light of mean field models, *Phys. Rev. D* **99**, 094028 (2019), [arXiv:1812.10380 \[hep-ph\]](#).
 - [52] S. Ghosh, N. Chaudhuri, S. Sarkar, and P. Roy, Effects of the anomalous magnetic moment of quarks on the dilepton production from hot and dense magnetized quark matter using the NJL model, *Phys. Rev. D* **101**, 096002 (2020), [arXiv:2004.09203 \[nucl-th\]](#).
 - [53] A. Yamamoto and Y. Hirono, Lattice QCD in rotating frames, *Phys. Rev. Lett.* **111**, 081601 (2013), [arXiv:1303.6292 \[hep-lat\]](#).
 - [54] W.-T. Deng and X.-G. Huang, Vorticity in Heavy-Ion Collisions, *Phys. Rev. C* **93**, 064907 (2016), [arXiv:1603.06117 \[nucl-th\]](#).
 - [55] M. Wei, Y. Jiang, and M. Huang, Mass splitting of vector meson and spontaneous spin polarization under rotation, (2020), [arXiv:2011.10987 \[hep-ph\]](#).